Design-oriented approach to determine FRC constitutive law parameters considering the size effect

Eduardo Galeote[a,] *, Ana Blanco[b], Albert de la Fuente[a]

[a]Department of Civil and Environmental Engineering, Universitat Politècnica de Catalunya, Jordi Girona 1-3, 08034 Barcelona, Spain

[b]School of Architecture, Building and Civil Engineering, Loughborough University, Loughborough, Leicestershire LE11 3TU, United Kingdom

* Corresponding author: Eduardo Galeote. Department of Civil and Environmental Engineering, Universitat Politècnica de Catalunya, Jordi Girona 1-3, 08034 Barcelona, Spain. Email address: eduardo.galeote@upc.edu

Abstract

Tensile strength constitutive laws for fibre reinforced concrete (FRC) are commonly defined through the parameters of flexural tests conducted on standard prismatic specimens. However, there are no specific criteria to determine such parameters using small specimens that could simplify the testing procedure and provide more representative results of slender structural FRC elements. In this line, the influence of size effect becomes an issue particularly relevant during the characterisation stage and needs to be regarded, given that the residual strength decreases while increasing the size of the element. Hence, the objective of this document is to propose a methodology to obtain the parameters of the constitutive law using the flexural strength results of small specimens. For this, the residual strength of FRC was determined by conducting three-point bending tests on prismatic notched beams of 40x40x160, 100x100x400 and 150x150x600 mm. An analytical model based on sectional analyses and aimed at reproducing the flexural strength of FRC was also developed to assess the results of the alternative methodology to determine the parameters for the constitutive law. The results show that an approach based on the rotation instead of the crack opening as the reference parameter to estimate the stresses for the constitutive law leads to results less influenced by the size effect.

1 INTRODUCTION

Size effect has been an issue extensively studied and reported in the literature, with different theoretical approaches arising to explain such effect. According to previous investigations, using specimens of different dimensions to determine the flexural response of fibre reinforced concrete (FRC) has several implications regarding size effect that may influence the nominal strength. While some studies [1] conclude that the size effect on the flexural strength is almost negligible, other researchers [2] state that the size effect cannot be disregarded. This issue was addressed in additional investigations [3] by analysing the residual strength of different sized concrete specimens with and without fibres and concluded that increasing the size of the specimen leads to a reduction in the strength [4].

Despite the evident presence of size effect on concrete, most of the design codes and standards currently into effect still assume that the behaviour of concrete follows the classical theories of elasticity and

plasticity [5]. In this regard, it is broadly accepted that both tensile and flexural strength capacities of concrete are not affected by the size effect at the structural design level. In the case of FRC, the fact of being a relatively new material for design purposes has also led to generally assume there is no size effect.

Among the existing codes and guidelines with specific FRC constitutive laws, only the German code (DBV) and the RILEM recommendations [6] account for the size effect by introducing a correction factor to reduce the strength as the size of the specimen increases [7]. Unlike the DBV and the RILEM specifications, the constitutive model for FRC of the *fib* Model Code 2010 (MC2010) [8] assumes an equivalent residual strength between the standard beam and the structural element. In this line, it has been reported [9] that the direct application of constitutive models on real-scale elements without considering the size effect may lead to an unsafe design given the influence of the geometry differences and the variations of the fibre distribution and orientation depending on the size of the element [10].

Constitutive models for the design of FRC real-scale elements are usually based on the results of standard prismatic beams tested under a three-point bending configuration. In this regard, this study aims to analyse whether small specimens may be used to determine the post-cracking parameters of FRC and which assumptions need to be taken for this purpose of guaranteeing the required reliability of the resulting design parameters. Hence, the cracking mechanism is analysed in detail to propose an approach based on replacing the crack mouth opening displacement (CMOD) for the rotation of the specimen as the reference parameter to determine the residual strength of FRC. The method consists of an inverse analysis to analytically compute the FRC flexural strength, which allows obtaining the load-deflection or load-crack opening curves by using the constitutive law of the MC2010. The analytical results are consequently compared to experimental results conducted on prismatic beams of different sizes (40x40x160, 100x100x400 and 150x150x600 mm) to determine which reference parameter—CMOD or rotation—presents the closest results to the experimental curves.

Finally, an alternative approach to assess the constitutive law for FRC using small non-standard specimens is proposed based on the obtained results. This approach can lead to simplify the testing procedure while providing more representative results for thin or slab-shaped FRC elements, which are commonly subjected to a greater influence of the preferential fibre orientation that takes place [11][12].

2 ANALYTICAL ASSESSMENT OF THE POST-CRACKING STRENGTH

2.1 Constitutive law for FRC

Different constitutive models in varying degrees of complexity and accuracy associated may be found in the literature and national or international codes for FRC [7] and even for ultra-high performance fibre reinforced concrete [13]. The main particularity of the stress-strain tensile law of the MC2010 for FRC with respect to other codes is that it can distinguish among three cases of softening and hardening behaviour (Fig. 1). The branches describing the strain-softening or strain-hardening post-cracking performance are defined by the stress and the strain at both Service and Ultimate Limit State (SLS and ULS). The stress parameters are calculated through the results of the three-point bending test (3PBT) conducted according to the standard EN 14651:2007 [14]. Based on the specifications of the MC2010, the strain may be obtained as the ratio between the crack opening and the characteristic length ($\varepsilon = w/l_{cs}$). At ULS, the MC2010 limits the strain (ε_{ULS}) to 10‰ in hardening and 20‰ in softening.

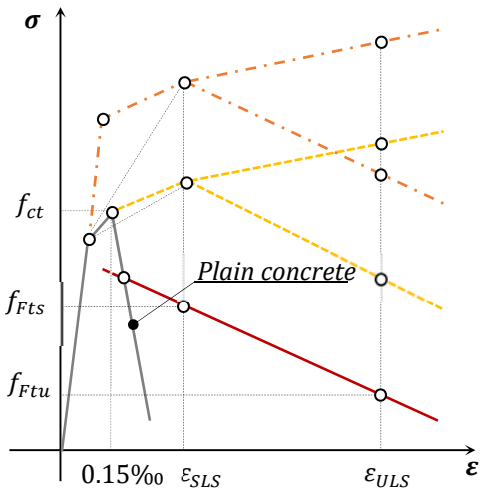

Figure 1. Constitutive law for FRC in tension [8].

The characteristic length (l_{cs}) is an indicator of the crack spacing used in calculations whose value is influenced by several factors such as the type or content of fibres, the matrix strength and the load level, among others [15]. Studies in the literature reveal that there is not a clear consensus to specify l_{cs} and researchers use different criteria to determine its value [15]. However, the MC2010 assumes l_{cs} to be equal to the depth of the element, which is used and validated by several authors [16][17].

2.2 Alternative approach to calculate the constitutive law for FRC

The 3PBT provides three strength values (f_{LOP}, f_{R1}, f_{R3}) which are used to calculate the parameters of the constitutive law f_{ct}, f_{Fts} and f_{Ftu} for FRC. These parameters are associated to specific CMODs of a standardized beam. However, the MC2010 lacks specific indications to calculate these parameters in case smaller non-standard specimens are used. The main issue lies in which CMOD should be considered when using smaller specimens to determine f_{Fts} and f_{Ftu}. This can be addressed by considering two approaches analysed through the simplified failure mechanism of a beam under a three-point bending test setup considering the mid-upper point as a hinge bonding the two halves of the specimen (Fig. 2).

The first approach, referred to as Full Crack Opening (FCO), is represented in Fig. 2a and assumes the use of the same crack opening for any specimen size, thus requiring smaller samples to achieve a greater rotation (θ_2) than larger samples (θ_1). The second approach, shown in Fig. 2b and named Equivalent Crack Opening (ECO), is based on the use of crack openings proportional to the beam depth. In such case, the equivalent CMOD of any specimen may be obtained through a relationship between rotation, crack opening and sample depth [18].

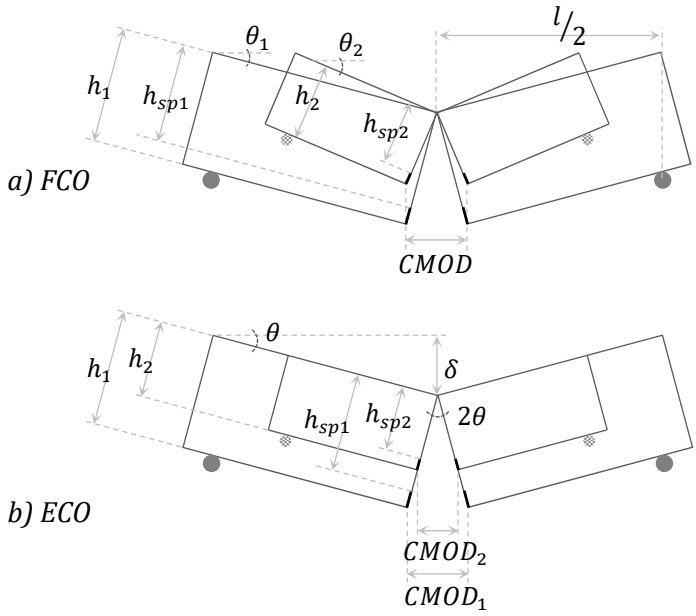

Figure 2. Failure mechanisms of the three-point bending test: a) FCO and b) ECO

According to the notation indicated in Fig. 2a, which considers $w = CMOD$ and $l_{cs} = h_{sp}$, the relation between the strains of different sized specimens in FCO approach can be deduced. Given that crack openings of both beams present the same absolute value, the CMOD of a smaller sample is proportionally wider than the CMOD of a larger sample, thus leading small specimens to present greater strains (Eq. 4).

$$\varepsilon_1 = \frac{CMOD}{h_{sp1}};\ \varepsilon_2 = \frac{CMOD}{h_{sp2}} \tag{1}$$

$$\varepsilon_1 h_{sp1} = \varepsilon_2 h_{sp2} \tag{2}$$

$$h_{sp1} > h_{sp2} \tag{3}$$

$$\varepsilon_1 < \varepsilon_2 \tag{4}$$

ECO approach assumes a constant rotation (θ) for any specimen size, thus leading to smaller CMODs and deflections (δ) in samples of smaller dimensions. This approach results in CMODs that are proportional to the depth of the specimen, leading to identical strains for the different sized beams (Eq. 8). The residual strengths f_{R1} and f_{R3} in specimens with non-standard dimensions calculated through ECO are, hence, those associated to sized-equivalent crack openings.

$$\varepsilon_1 = \frac{CMOD_1}{h_{sp1}};\ \varepsilon_2 = \frac{CMOD_2}{h_{sp2}} \tag{5}$$

$$\theta = \frac{CMOD_1}{2h_{sp1}} = \frac{CMOD_2}{2h_{sp2}} \tag{6}$$

$$\varepsilon_1 = 2\theta;\ \varepsilon_2 = 2\theta \tag{7}$$

$$\varepsilon_1 = \varepsilon_2 \tag{8}$$

Given that the crack opening is assumed to remain constant for different specimen dimensions with FCO, ε_{SLS} and ε_{ULS} decrease while the sample size increases. Conversely, according to ECO, ε_{SLS} and

ε_{ULS} present identical values for different specimen dimensions due to the use of proportional crack widths and h_{sp}. As a result of the proportionality between the crack opening and h_{sp}, crack openings calculated through ECO increase linearly with the specimen dimension. These variations of strain in FCO and crack opening in ECO are shown in Fig. 3.

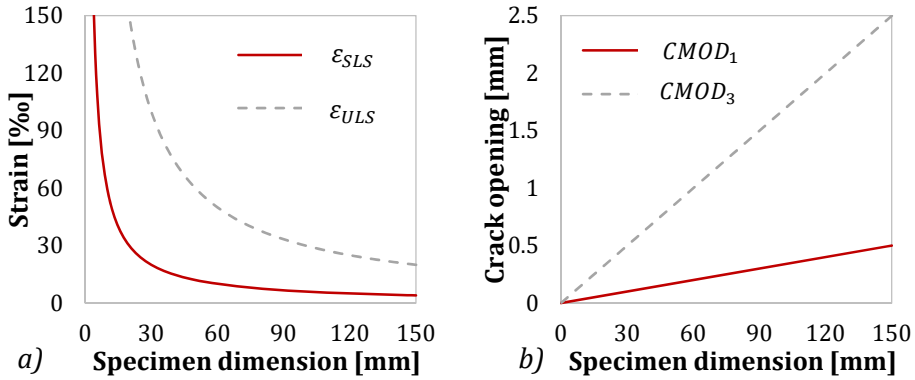

Figure 3. a) Strain according to FCO and b) crack opening with ECO.

2.3 Analytical procedure

A back-calculation based on an analysis of evolutionary sections (AES) [19][20] with a multi-layer approach was used to obtain analytically the flexural behaviour of FRC. Given its simplicity and accuracy, similar methods have also been used by several researchers [21]–[26]. To conduct the AES, several assumptions were adopted:

(i) Sections remain plane after loading or imposed strains (hypothesis of Navier-Bernoulli).

(ii) Strain compatibility: perfect bond between concrete and fibres is assumed.

(iii) Shear distortion and stresses are negligible and were not considered (hypothesis of Euler-Bernoulli).

(iv) Internal forces are applied on the symmetrical axis of the section.

The material properties in compression and tension are defined through the constitutive law of the MC2010. In the analysis, the cross-section is discretised along its height into layers, and it is assumed that tensile stresses are located at the bottom whereas compression stresses are placed at the top part of the section. The bottom layer of the section is taken as reference for the analysis, where a tensile strain ε_{bot} is assumed for the initial stage. Subsequently, a compressive strain at the top (ε_{top}) is assumed so the curvature χ and the strain at any layer may be calculated through Eq. 9 according to the combination of Navier-Bernouilli hypothesis with the strain compatibility assumption. A schematic representation of the discretization and the linear strain distribution is represented in Fig. 4.

$$\chi = \frac{\varepsilon_{top} - \varepsilon_{bot}}{h} = \frac{\varepsilon_{top} - \varepsilon(z)}{z} \tag{9}$$

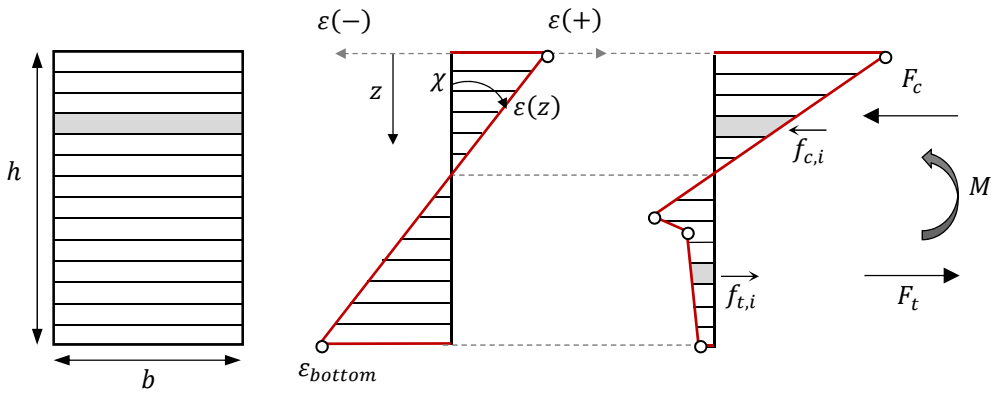

Figure 4. Schematic discretisation of the cross-section and the distributions of strains and stresses.

The equilibrium condition between the internal and the external forces is satisfied by imposing Eqs. 10 and 11. For this, the predefined constitutive stress-strain law is used to calculate the stresses out of each strain from the linear distribution. The forces at each layer are calculated through the stresses and are assumed to be applied at the mid-thickness of its corresponding layer.

$$N = \int_{A_c} f_{c,i} dA_{c,i} + \int_{A_c} f_{t,i} dA_{c,i} \tag{10}$$

$$M = \int_{A_c} z f_{c,i} dA_{c,i} + \int_{A_c} z f_{t,i} dA_{c,i} \tag{11}$$

If the equilibrium condition is not verified, a new ε_{top} is assumed and iterated until the equilibrium is satisfied. At this stage, the internal flexural moment at the section may be calculated. Additionally, the crack opening can be obtained through the strain at the bottom layer and the characteristic length ($w = \varepsilon \cdot l_{cs}$).

The steps for computing are shown in the flowchart of Fig. 5, using a similar procedure to the one described in previous studies [24][27]. The method begins assuming an initial strain at the bottom fibre and calculates the strains at the cross-section by an iterative process checking whether the equilibrium conditions are satisfied. When a result is achieved, the strain at the bottom increases and the iterative process starts over.

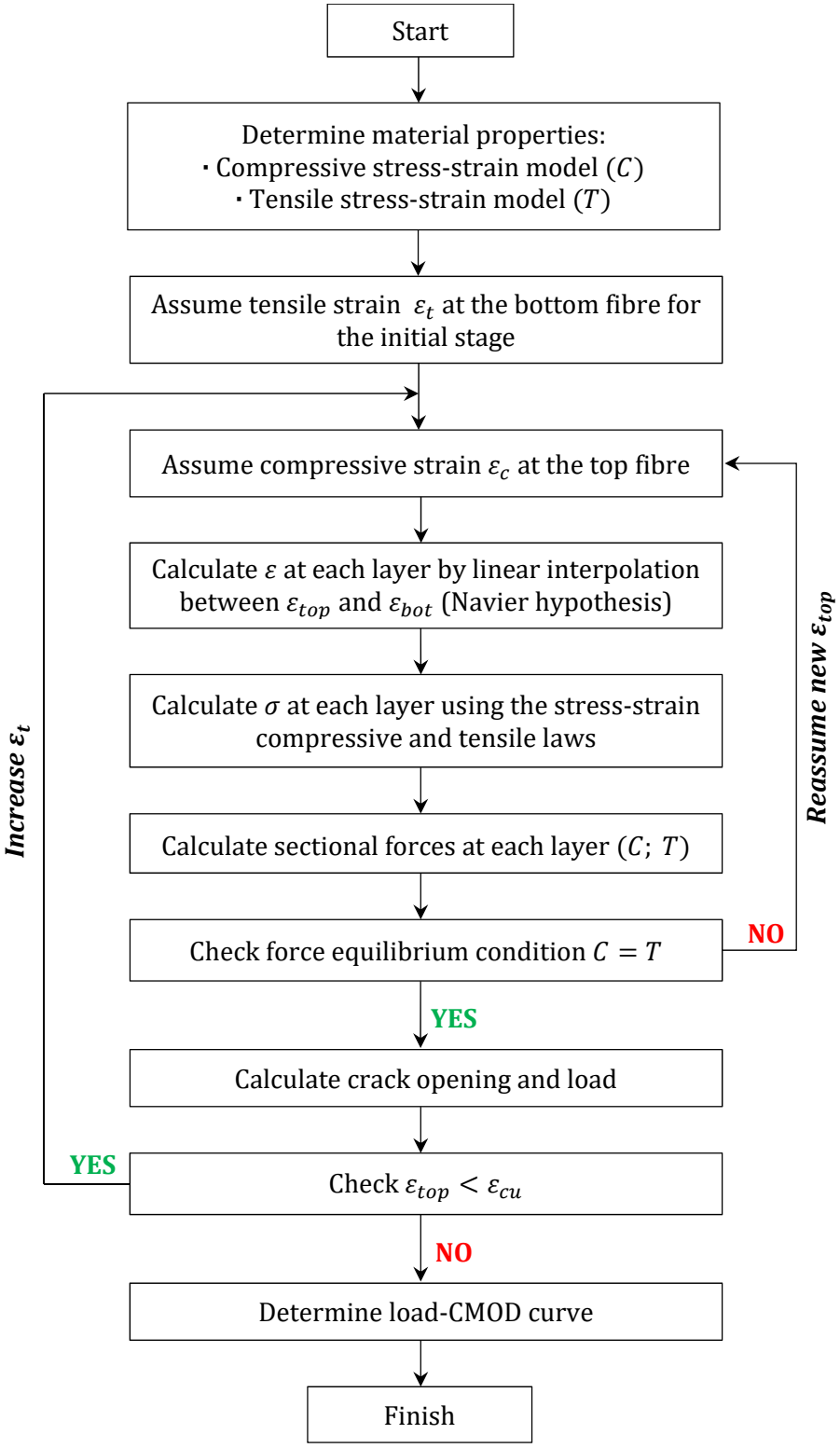

Figure 5. Flow chart of the analytical cross-sectional model.

3 EXPERIMENTAL PROGRAM

3.1 Materials and concrete mixes

One plain concrete mix (M0) and four high-performance fibre reinforced concrete mixes with contents of 90 and 190 kg/m^3 of steel straight microfibres ($l = 13\ mm$, $\phi = 0.20\ mm$ and $f_{yu} = 2750\ MPa$) were produced (Table 1). As in other studies [28], the content of fibres was increased by replacing an equivalent volume of silica sand to keep constant the content of cement.

Nanosilica was introduced in all mixes as a highly reactive pozzolanic material in a content of 5% over the cement weight (o.c.w.) to enhance the strength. Based on the results of previous research [29], powders with high specific surface increase the water demand to maintain workability, which has a direct influence on the content of water and superplasticizer. Accordingly, mixes M0, M90A and M190A have a lower amount of water than mixes M90B and M190B, which was compensated with a greater content of superplasticizer.

Table 1. Concrete mixes.

Materials	M0	M90A	M190A	M90B	M190B
CEM I 52.5R	800	800	800	800	800
Silica sand 3 – 4 mm	1161	1131	1098	1129	1098
Filler ($CaCO_3$)	200	200	200	200	200
Water	129	129	129	185	185
Nanosilica (o.c.w.)	5%	5%	5%	5%	5%
Superplasticizer (o.c.w.)	4%	4%	4%	2%	2%
Steel fibres	0	90	190	90	190

3.2 Concrete production and specimens

The concrete was produced using a vertical axis mixer with an automatized system to weight and introduce the dried materials with the specified amount of water. The nanosilica, the superplasticizer and the fibres were introduced to the mix manually through an opening on the mixer. After mixing, the concrete mix was directly poured from the skip to the moulds. A curing layer was sprayed over the free surface of the specimens to prevent the loss of superficial water and a consequent early shrinkage.

For each concrete mix, 3 cubic specimens of $150x150\ mm$ and 3 cylindrical $\phi 150x300\ mm$ samples were produced. Moreover, 3 prismatic samples with dimensions of $150x150x600\ mm$, 6 samples of $100x100x400\ mm$ and 9 samples of $40x40x160\ mm$ were cast, thus resulting in a total amount of 108 prismatic beams of three dimensions. The use of microfibres was necessary given that the small specimens limit the size of the fibres. The cubic specimens were used to perform compressive tests according with EN 12390-3 [30], the cylindrical samples to assess the modulus of elasticity following the indications of EN 12390-13 [31] and the prismatic specimens to determine the flexural and residual strength through the three-point bending test based on the standard EN 14651 [14].

The dimensions of the specimens for the three-point bending test, as specified in EN 14651, are prisms of $150x150x600\ mm$. To conduct the tests with smaller specimens $100x100x400$ and $40x40x160\ mm$, the notch depth and the span length had to be adjusted according to the dimensions of these samples. Following previous research [32][33][34], the depth-span and depth-notch ratios of

the $150x150x600\ mm$ beams were kept constant to maintain the proportions between the dimensions of the beams. Table 2 shows the effective depth (h_{sp}) and the span of the three different prisms sizes.

Table 2. Characteristic dimensions of the specimens for the three-point bending test.

Specimen dimension [mm]	Effective depth h_{sp} [mm]	Span [mm]
$150x150x600$	125.0	500
$100x100x400$	83.3	333
$40x40x160$	33.3	133

4 ANALYSIS OF RESULTS

4.1 Compressive strength and modulus of elasticity

The average results of the compressive strength for three different sized cubic specimens and the results of the modulus of elasticity performed on standard cylindrical samples are detailed in Table 3.

Table 3. Results of compressive strength and modulus of elasticity.

Mix	Compressive strength [MPa]						Modulus of elasticity [MPa]	
	150x150 mm		100x100 mm		40x40 mm		ϕ150x300 mm	
	Average	CV	Average	CV	Average	CV	Average	CV
M0	111.2	1.8%	96.9	2.0%	97.4	7.2%	36429	0.5%
M90A	115.9	0.7%	109.5	2.9%	126.8	8.4%	36337	0.5%
M190A	117.2	0.5%	115.0	3.4%	133.6	6.4%	37674	0.5%
M90B	108.8	2.4%	102.1	1.6%	122.8	7.9%	32807	0.3%
M190B	100.3	6.8%	103.3	1.9%	124.9	6.4%	34095	9.3%

A comparison between FRC mixes with different water-cement ratios (w/c) confirm an expected reduction of the compressive strength for higher w/c ratios. This effect may also be appreciated in the modulus of elasticity, with lower values for higher w/c ratios. The higher content of water in the mix with greater w/c ratios is the main responsible of inducing a higher porosity in the concrete matrix and, therefore, reducing both the compressive strength and the modulus of elasticity.

In line with the results reported in other studies [35]–[37] the addition of fibres slightly increased the compressive strength except mixes M90B and M190B, which presented a reduction of the compressive strength from 108.8 to 100.3 MPa. This generalised increase of strength may be attributed to a certain confinement effect of the microfibers, inhibiting and delaying microcracking propagation produced by compression stresses when above $0.4f_{cm}$.

4.2 Flexural strength

The average flexural strengths of the three-point bending tests conducted on $150x150x600\ mm$ specimens are shown in Table 4. The values show the strengths at the limit of proportionality (f_{LOP}) and at CMODs of 0.5, 1.5, 2.5 and 3.5 mm (f_{R1}, f_{R2}, f_{R3} and f_{R4}). These results were calculated as described in the standard EN 14651.

Table 4. Average flexural strengths of M90A, M190A, M90B and M190B.

Flexural strength	M90A		M190A		M90B		M190B	
	Average [MPa]	CV [%]	Average [MPa]	CV [%]	Average [MPa]	CV [%]	Average [MPa]	CV [%]
f_{LOP}	8.02	6.5	9.54	6.8	7.86	2.3	8.16	-
f_{R1}	14.58	5.8	17.83	7.6	12.06	6.9	16.35	-
f_{R2}	14.63	4.0	16.96	2.7	11.99	4.0	15.75	-
f_{R3}	13.03	3.8	14.73	4.6	10.36	3.9	13.00	-
f_{R4}	11.18	3.7	11.99	4.3	8.69	3.6	10.37	-

Increasing the content of fibres from 90 to 190 kg/m^3 enhanced f_{LOP} especially from mix M90A to M190A, with M190A presenting a f_{LOP} approximately 15% higher than M90A. These results are similar to those reported in previous studies using microfibres [38]. In line with the results of other researchers [39], a comparison of f_{LOP} of mixes M90A, M90B and M190B presents a variation of only 1.9% given that f_{LOP} is mainly influenced by the properties of the matrix and the w/c ratio [40][41].

The post-cracking results exhibited expected trends according to the content of fibres and the w/c ratios. In both groups of mixes (A and B), the increasing amount of fibres entailed a greater residual strength while the reduction of the w/c ratio led to lower bending stresses. Notice also that the scatter of the residual strengths is considerably low in comparison with the results of other studies [41][42]. This is mainly attributed to the higher fibre density in the cracked surface [35][43] which provides a higher homogeneity to flexural stresses.

The average flexural strength is expressed in terms of strength-rotation curves in Fig. 6. The use of the rotation as an alternative parameter to CMOD when different sized specimens are compared has also been supported by other authors [18].

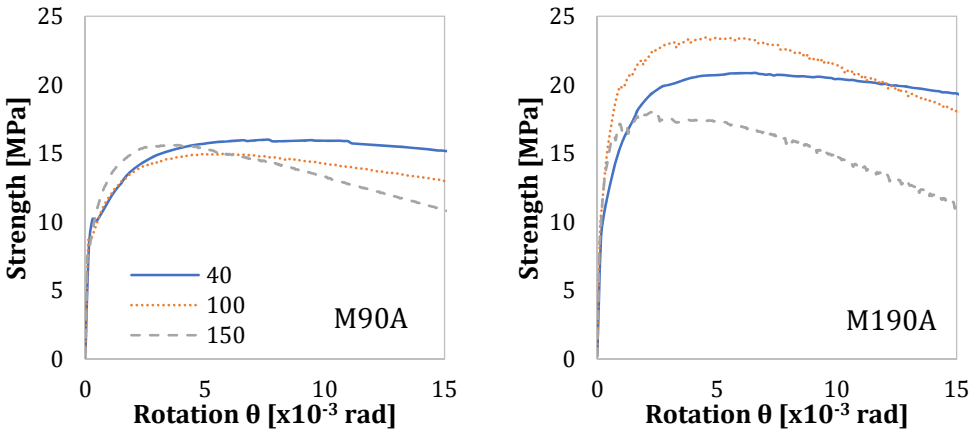

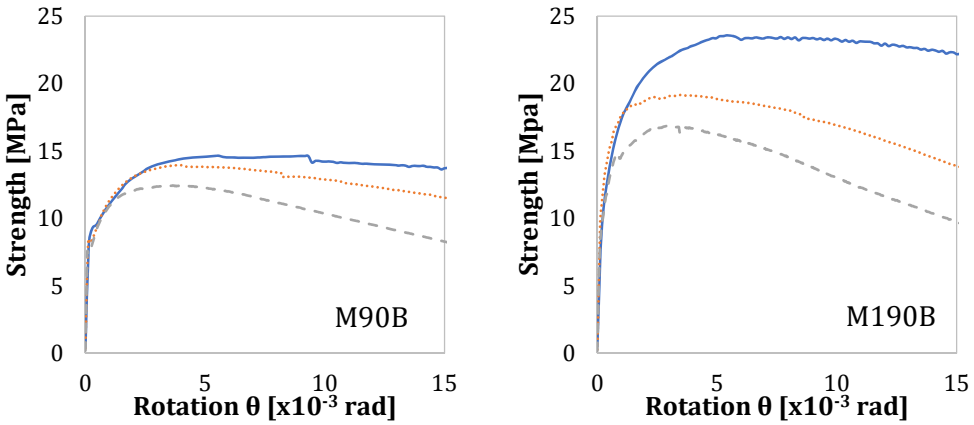

Figure 6. Average flexural stress in terms of strength-rotation.

All mixes exhibit a rotation-hardening behaviour and a clear influence of the specimen size on the residual strength. As shown by other authors [44], the strength in mixes M90B and M190B decreased as the specimen size increased. However, such a clear trend between the strength and the size of the specimen could not be identified in mixes M90A and M190A. In M90A, similar results were obtained for the three sizes of specimens up to a rotation of $0.006\ rad$. From this point onwards, the residual strength shows a behaviour inversely proportional to the dimension of the element as in the case of mixes M90B and M190B.

The observations in M190A differ with the findings of previous studies [4][45] with similar contents and types of fibres. Nonetheless, M190A was produced with a considerably low w/c ratio and a high content of fibres (0.16 and 190 kg/m^3, respectively) in comparison to the aforementioned studies. The combination of these two variables results in a lower flowability of concrete [46], which directly affects the orientation of the fibres in the element and the flexural strength [47].

The average f_{LOP} and the average maximum strength of the four mixes are shown in Fig. 7 represented according to the specimen size. The general trend indicates a reduction of both strengths while increasing the dimension of the specimen.

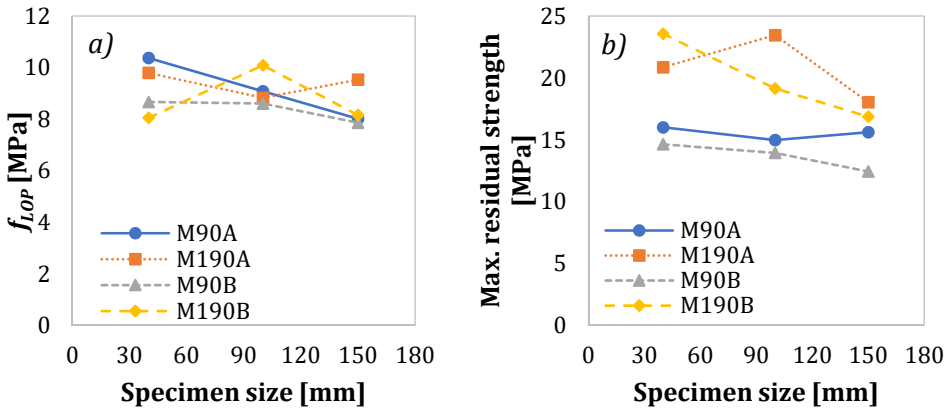

Figure 7. Size effect on a) f_{LOP} and b) maximum strength.

The results of the 40x40x160 mm specimens in Fig. 7a confirms the minor influence of the content of fibres on f_{LOP}, showing that the w/c ratio is the main responsible of the differences in the cracking strength. The lower strength of mixes with 190 kg/m^3 with regard to their counterpart with 90 kg/m^3 confirms that increasing the content of fibres does not necessarily lead to a greater cracking strength. Indeed, the lower results of mixes M190A and M190B with regard to M90A and M190B, respectively,

may be a consequence of a higher induced porosity in the matrix as a result of the higher content of fibres [48], [49]. Increasing the content of fibres enhanced the maximum residual strength (Fig. 7b), which is a direct effect of the greater number of fibres in the cracked section [47], [50]. These results also indicate that a lower w/c ratio improved the bond strength at the fibre-matrix interface [51].

4.3 Constitutive models

The constitutive model for FRC was calculated for each mix and specimen dimension to conduct the analytical calculations, obtaining both ε_{SLS} and ε_{ULS} following the relation between crack opening and strain of the MC2010. Considering the characteristic length l_{cs} of each specimen as the effective depth h_{sp}, CMODs and strains at SLS and ULS for each approach analysed (FCO and ECO) take the values shown in Table 5.

Table 5. Crack openings and strains, according to FCO and ECO.

Specimen dimension	Full crack opening (FCO)				Equivalent crack opening (ECO)			
	$CMOD_1$ [mm]	$CMOD_3$ [mm]	ε_{SLS} (‰)	ε_{ULS} (‰)	$CMOD_1$ [mm]	$CMOD_3$ [mm]	ε_{SLS} (‰)	ε_{ULS} (‰)
40 mm	0.50	2.50	15.00	75.00	0.13	0.67	4.00	20.00
100 mm	0.50	2.50	6.00	30.00	0.33	1.67	4.00	20.00
150 mm	0.50	2.50	4.00	20.00	0.50	2.50	4.00	20.00

Both strengths f_{Fts} and f_{Ftu} of the constitutive law are calculated for each geometry at $CMOD_1$ and $CMOD_3$, respectively. Given that the crack openings for both approaches are different, f_{Fts} and f_{Ftu} result in different values if calculated for FCO or ECO. A comparison between the constitutive laws for the three specimen dimensions according to FCO and ECO and the experimental results expressed in terms of strength-rotation are shown in Table 6.

Table 6. Constitutive laws, according to FCO and ECO and experimental results.

Mix	Full Crack Opening (FCO)	Equivalent Crack Opening (ECO)	Experimental result
M90A	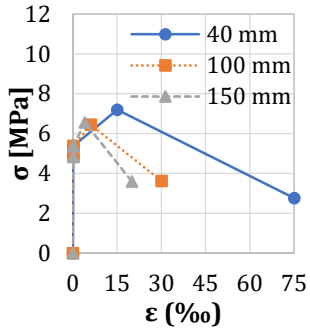	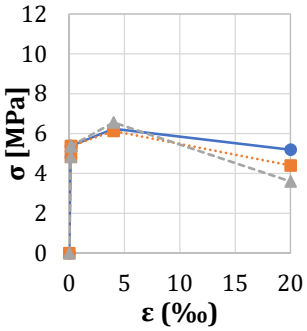	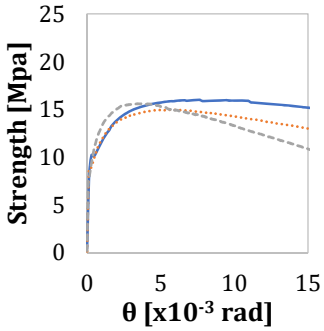

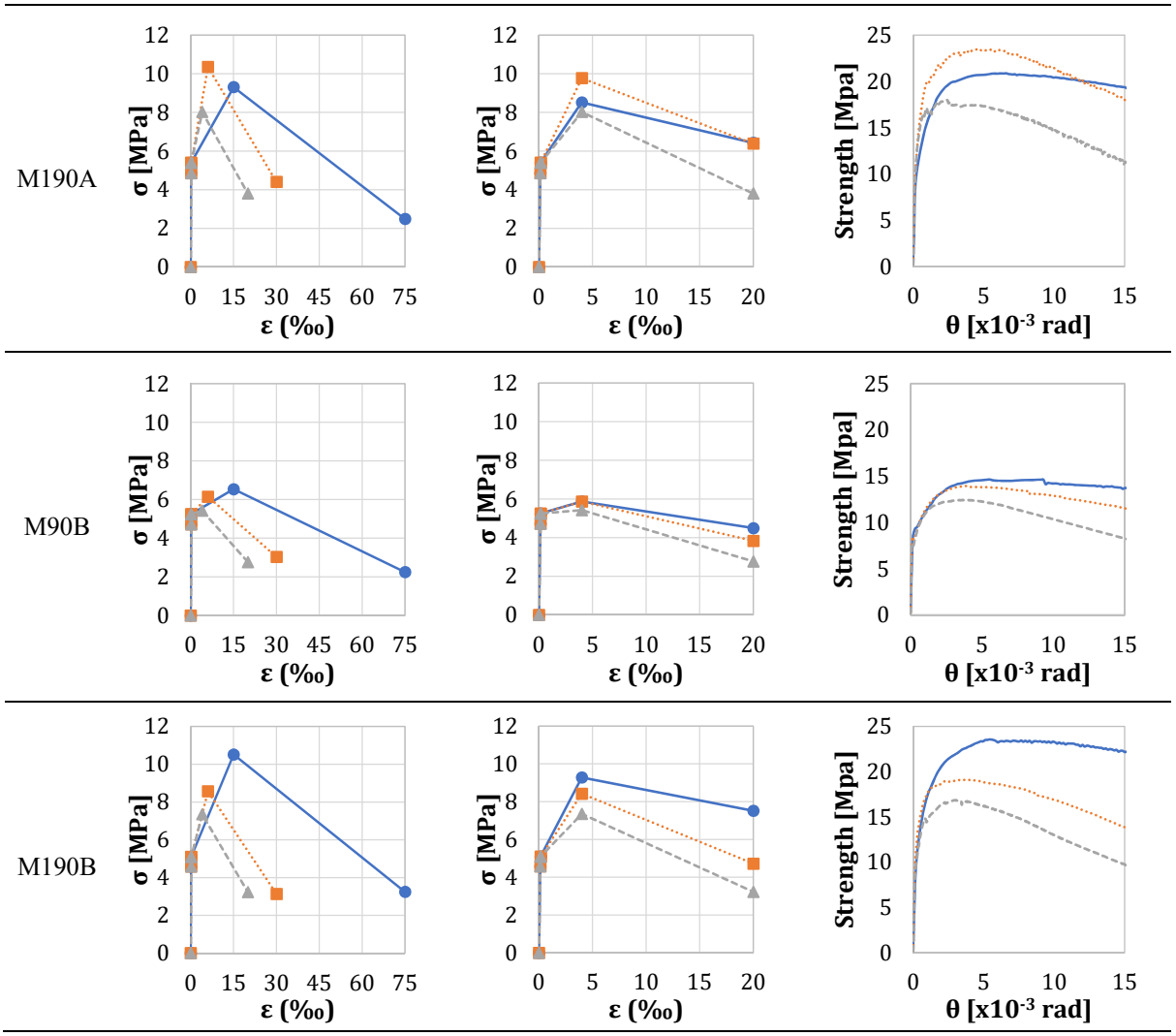

The main difference between both approaches lies in the strains at SLS and ULS. The greater strains in smaller specimens due to the proportionally higher crack opening are evidenced in the shape of the constitutive model calculated through FCO, this presenting lower strains at both SLS and ULS while increasing the specimen dimension. This result contrasts with the results of the constitutive model determined with ECO since the crack openings for each specimen dimension are proportional to the specimen size, and the strains remain constant regardless of the dimension of the element.

The constitutive model curves calculated with both approaches follow similar trends with smaller specimens showing greater strengths. A comparison of the experimental strength-rotation results with the constitutive laws indicates a greater resemblance of the experimental strength-rotation to the constitutive model calculated through ECO than the one determined with FCO. This is mainly caused by the two defining parameters: the strains and the stresses of the constitutive model, given that the assumptions of ECO entail that the rotation θ and the strain ε are directly proportional.

The strength parameters f_{Fts} and f_{Ftu} of the 4 mixes calculated according to both FCO and ECO for the three specimen sizes are shown in Fig. 8. The results reveal that the influence of the fibre content is more evident in f_{Fts} than in f_{Ftu}, this suggesting that the reinforcing effect of the micro-steel fibres under analysis is greater at reduced strains and crack openings and even greater in smaller specimens than in large samples. According to FCO approach in specimens of 40 mm, M190A and M190B present f_{Fts} values around 30% and 60% higher than M90A and M90B, respectively. These results contrast

with the counterpart in specimens of 150 mm, whose f_{Fts} variation for FCO changes from 30% to 22% and from 60% to 36%.

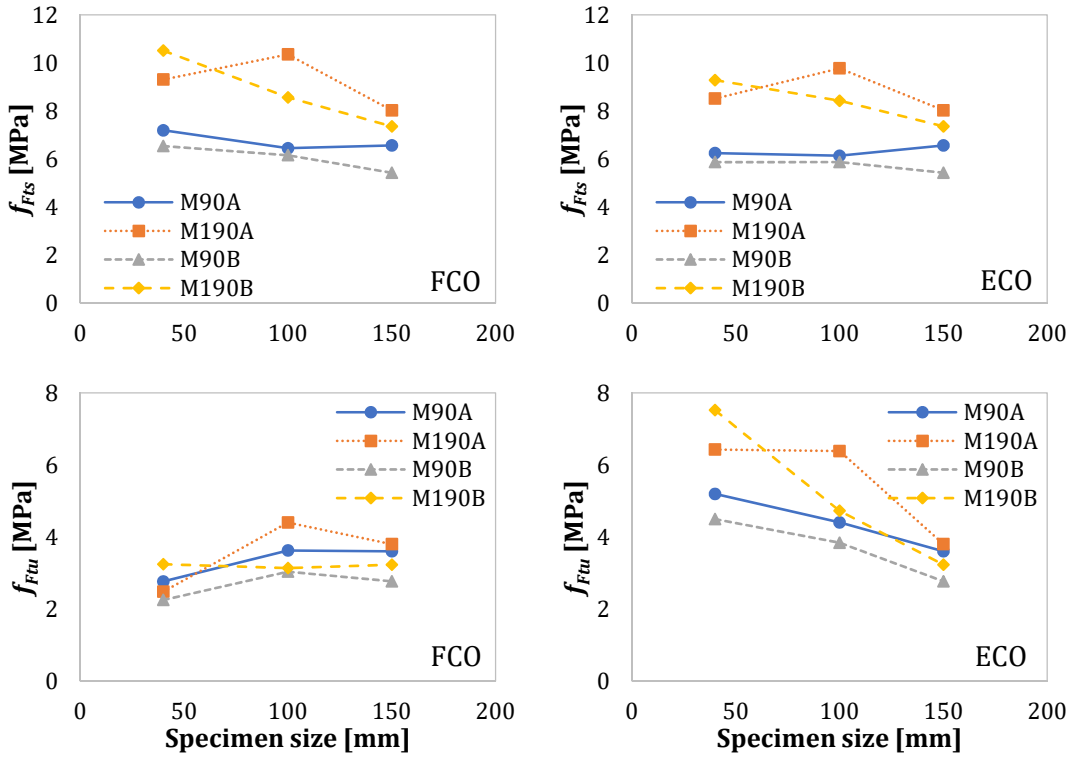

Figure 8. Size effect on f_{Fts} and f_{Ftu} according to FCO and ECO approaches.

A comparison between both approaches shows a strong similarity between FCO and ECO in terms of f_{Fts}, although there are relevant differences between approaches in f_{Ftu}. In the case of FCO, f_{Ftu} presents a slightly increasing trend as the dimensions of the samples increase. Conversely, f_{Ftu} exhibits a clear decreasing trend with the specimen size when calculated according to ECO approach. In this regard, f_{Ftu} presents considerably lower values for FCO than ECO in specimens of 40 mm.

4.4 Sectional analysis

Based on the constitutive models of Table 6, a comparison between the experimental curves of the four mixes and the analytical curves obtained with AES is shown in Fig. 9. The results are shown in terms of strength-rotation up to $\theta = 0.02\ rad$, which corresponds to a strain at the notch $\varepsilon = 40‰$. Notice that in specimens of 150 mm only one analytical curve is presented since for this dimension both FCO and ECO constitutive curves coincide. These results reveal that the analytical strength-rotation curves present a more accurate fitting when determined according to the ECO approach.

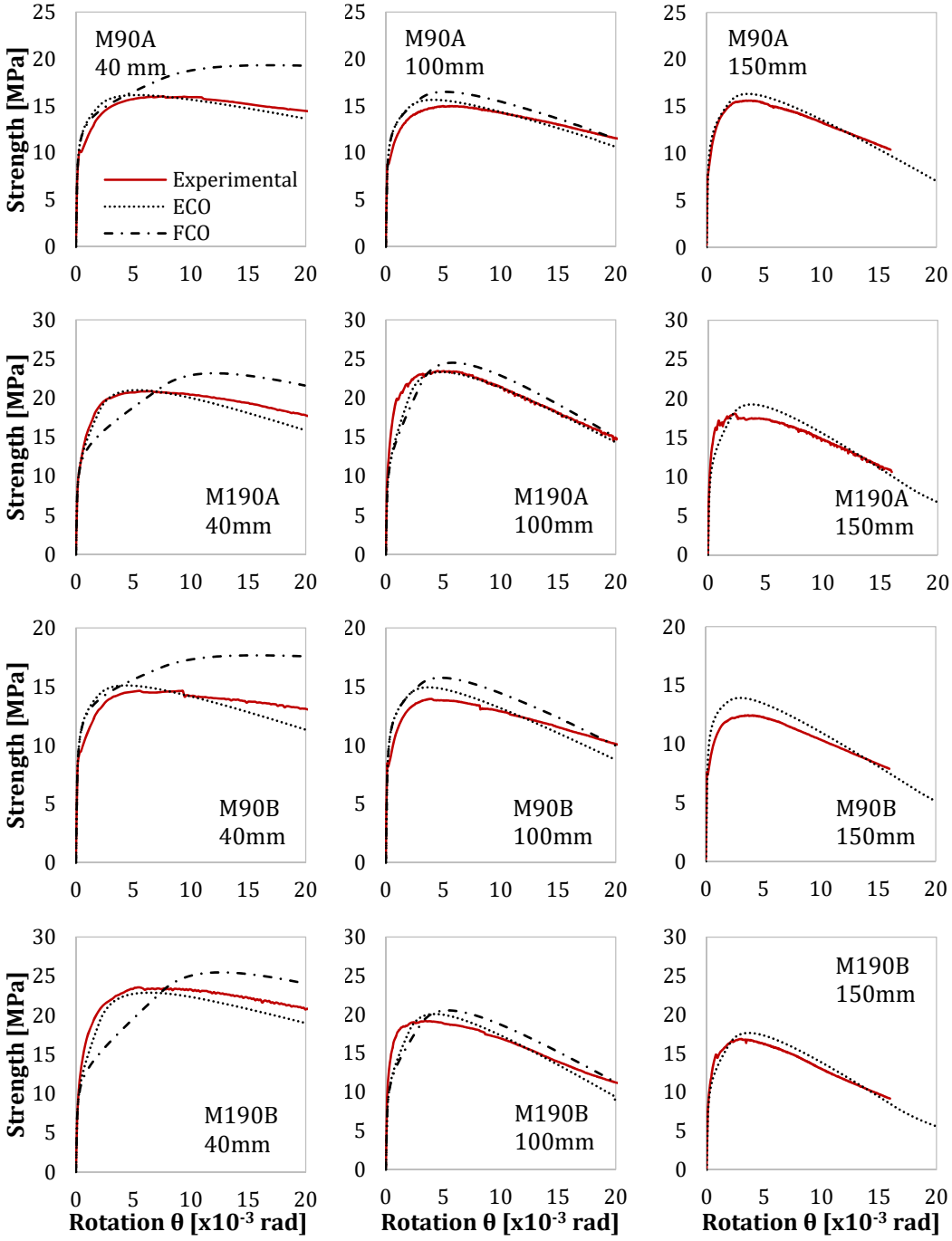

Figure 9. Comparison between experimental and MC2010 results.

There are no significant differences between approaches and the experimental results up to the cracking point since up to this point the constitutive law is defined according to the tensile strength of plain concrete and both approaches share the same parameters. From this point onwards, and at the cracked stage, the differences between the experimental and the analytical results are greater when using the FCO approach. These differences for FCO increase for higher contents of fibres and smaller specimens.

The differences between FCO and experimental results at small rotations are bigger for mixes with 190 kg/m^3, if compared with mixes blended with 90 kg/m^3. At $\theta = 3.5 \cdot 10^{-3}\ rad$, FCO yields a 15% lower strength for M190A than the experimental result, whereas the difference at the same rotation between ECO and the experimental values is only 1.5%. At $\theta = 20 \cdot 10^{-3}\ rad$, the differences with

respect to the experimental results were 21% (FCO) and 11% (ECO). As in the case of mixes with 90 kg/m^3, mix M190B presented analogous results to M190A.

For specimens of 40 mm and mix M90A, FCO and ECO presented a strength compared to the experimental results 2.8% and 5.2% higher at $\theta = 3.5 \cdot 10^{-3}\ rad$, respectively. At $\theta = 20 \cdot 10^{-3}\ rad$, the strength with FCO approach increased from to 33%, whereas the difference in ECO at this rotation remained 5.6% below the experimental value. Similar trends and results are obtained with mix M90B.

In specimens of 100 mm, the differences between analytical and experimental results shrank. Almost identical results were obtained with FCO and ECO up to a rotation of approximately $\theta = 2.5 \cdot 10^{-3}\ rad$ in M90A, overestimating the experimental results at this rotation in 8.7% and 8.5%, respectively. Regardless of the similarities between approaches, at greater rotations FCO provides higher strengths than both ECO and the experimental curve at greater rotations. In mixes M190A and M190B, both FCO and ECO present again similar results although underestimate the experimental value up to a rotation that corresponds approximately to the maximum flexural strength. After this, ECO presents more accurate results than FCO, which again slightly overestimates the results of the descending branch of the curve.

The analytical curve in specimens 150 mm represents both FCO and ECO approaches. It shows a reasonable fitting, albeit it overestimates the results if compared to the experimental values. The most accurate fitting occurs for M90A, while the greatest overestimation takes place in M90B.

4.5 Neutral axis and stress distributions

The results of the AES provide the strains at the bottom and at the top layer of the section to determine the neutral axis depth assuming the hypothesis of Navier-Bernouilli. The stress distributions and the relative position of the neutral axis to the specimen depth (x_n/h) obtained through the AES for a CMOD of 0.5 mm and a rotation of $5 \cdot 10^{-3}\ rad$ are shown in Fig. 10.

The results reveal the influence of the control parameter (CMOD or rotation) on the relative depth of the neutral axis depth x_n/h based on the strains and stresses patterns that satisfy the sectional equilibrium. If the crack opening is set to a certain CMOD regardless of the dimension of the specimen, the neutral axis leads to a lower x_n/h while the size of the element decreases given that ε_{bot} is greater due to the relation between the crack opening and the effective depth of the specimen ($\varepsilon = w/l_{cs}$), thus shifting the neutral axis upwards the cross-section with regard to larger samples (see Fig. 10). Conversely, a constant rotation θ entails an identical ε_{bot} regardless of the dimension of the element given that the strain is determined as a function of the rotation ($\varepsilon = \theta/2$). This leads to the same relative position of the neutral axis x_n/h when using elements with different effective depths.

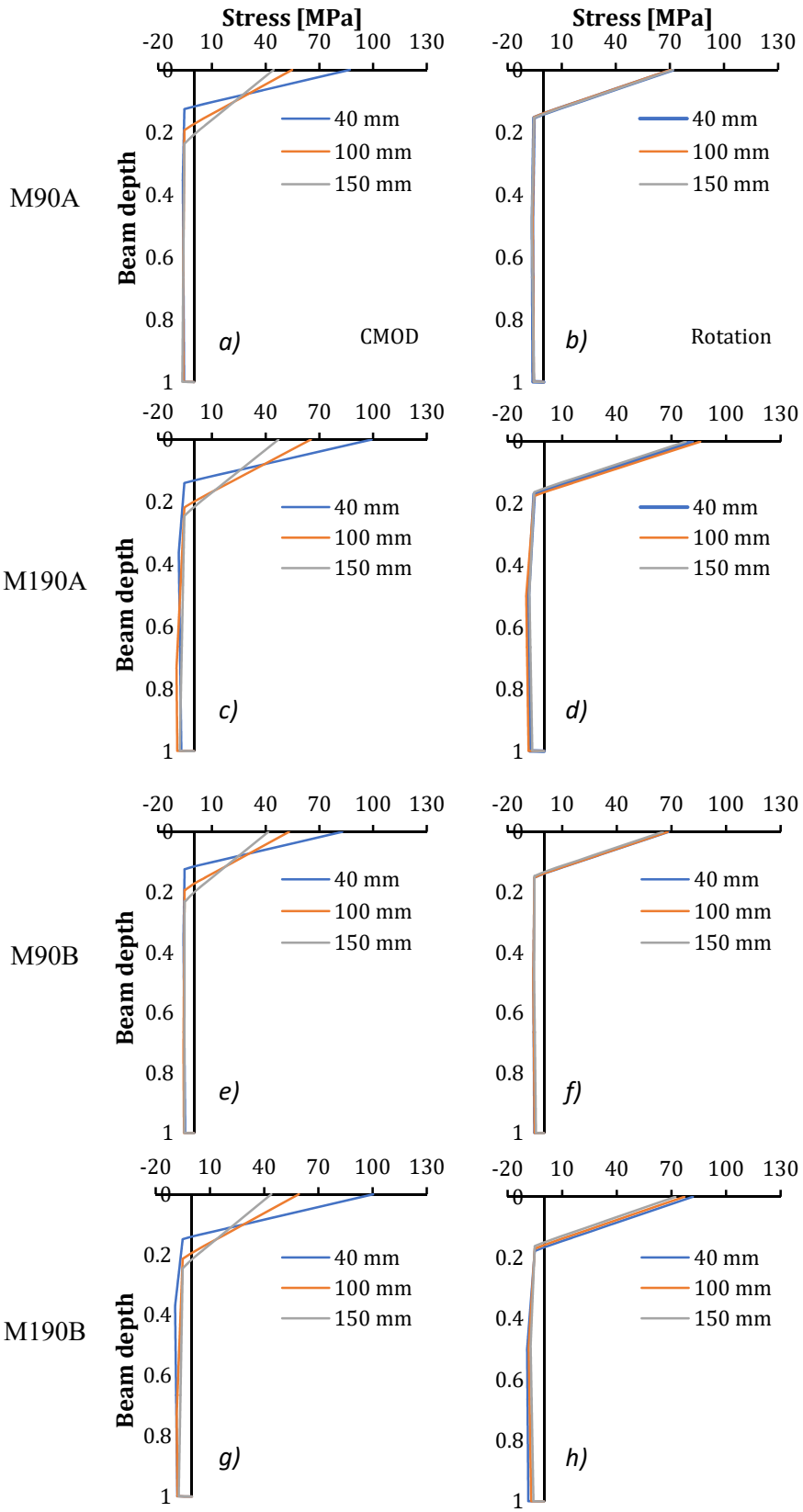

Figure 10. Stress distribution at the cross-section and relative neutral axis depth.

The position of the neutral axis x_n/h is extended to additional values of CMOD (FCO) and rotation (ECO) for different flexural levels (Fig. 11) for mix M90A. For the rest of the three mixes, similar curves might be obtained given the slight differences in the neutral axis depth results shown in Fig. 10.

Three curves—one for each specimen dimension—are obtained for both types of control: CMOD and rotation.

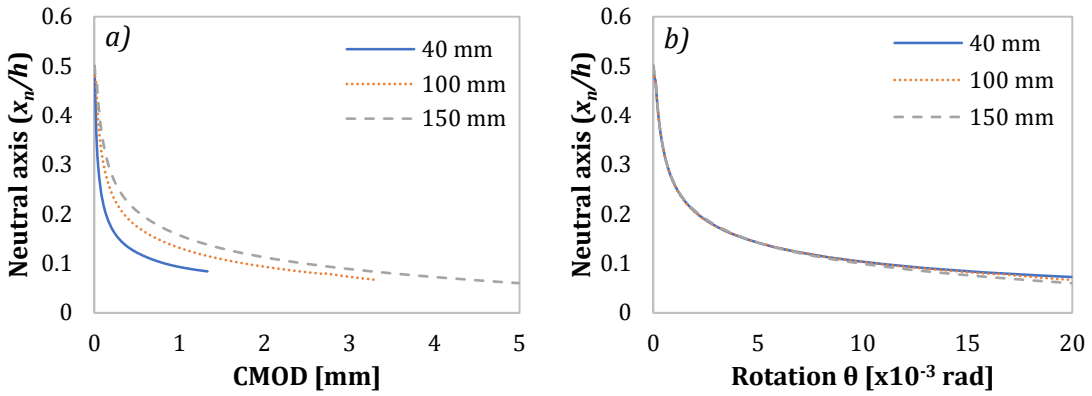

Figure 11. Neutral axis depth according to a) CMOD and b) rotation.

The dependence on the size of the element is greater for FCO given that the strain for a given CMOD is higher in smaller specimens, shifting the neutral axis upwards the section. The slight variation of x_n/h vs. rotation with the specimen size basically lies in the different shape of the constitutive law. In this case, a given rotation entails the same strain, but the stress at the constitutive law associated with that strain may be different depending on the size of the specimen.

The influence of the fibre content on the sectional stress distribution and the neutral axis at the mid-span cross-section of $150\ mm$ beams of the four mixes on a CMOD of $0.5\ mm$ and a rotation $\theta = 0.002\ rad$ is shown in Fig. 12.

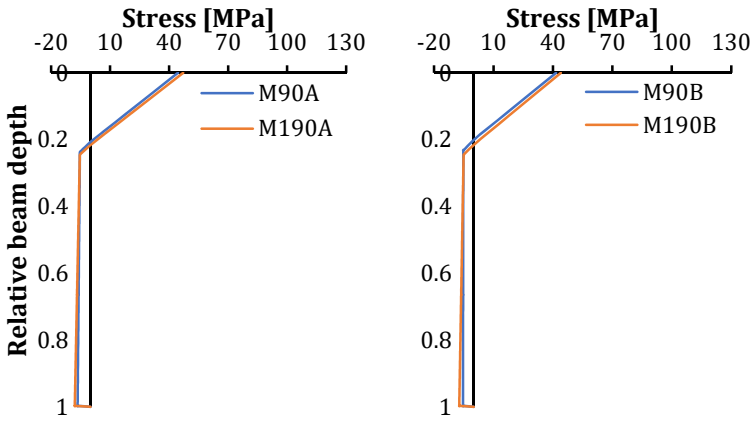

Figure 12. Neutral axis depth according to the content of fibres.

Notice that for this specific case of study, insignificant differences may be observed in x_n/h when comparing the results according to the content of fibres. This is in line with the results of previous studies [52], which show that the position of the neutral axis is barely influenced by the content of fibres when the volume of fibres in the concrete mix exceeds a volume of 1.0%. However, these results may not be applicable to other cases given that the position of the neutral axis does not only depend on the type and content of fibres, but also on the compressive strength and the resulting equilibrium of forces at the sectional analysis.

According to this experience, the contents of fibres below 1.0% would lead to decreasing x_n/h. A comparison of the content of fibres throughout further rotations is shown in Fig. 13, showing the scarce differences in x_n/h attributed to the content of fibres.

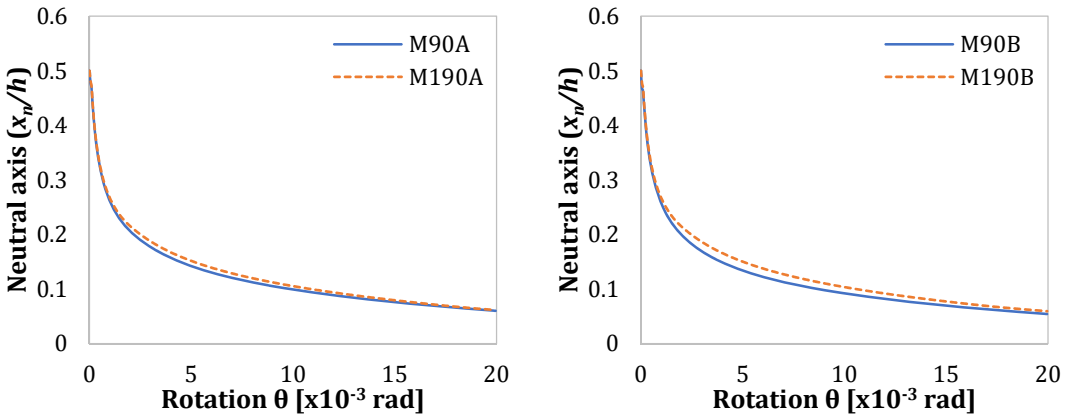

Figure 13. Extended neutral axis depth-rotation according to the content of fibres.

5 CONCLUSIONS

This study confirms the influence of the dimension of the specimens on the flexural strength and proposes an alternative approach to determine the parameters of the constitutive law for FRC based on the specifications of the MC2010. The conclusions are drawn from this study state as follows:

- Using the rotation as a reference parameter (ECO) instead of the CMOD (FCO) to define the parameters of the constitutive tensile laws leads to an improved numerical fitting of the experimental results and reduces the specimen size dependence. Strains and crack openings are comparatively larger in small specimens than in standard ones when calculated according to FCO, whereas ECO provides proportional CMODs to the size of the specimen and constant strains.
- Reducing the size of the element may present advantages in terms of representativeness for slender structures or elements produced with high strength concrete that allow reducing cross-section dimensions and are subjected to a greater influence of the fibres due to preferential orientations.
- Quality control procedures can be simplified, given that the reduction of the dimensions of the samples leads to lighter and more manageable specimens. Three 100x100x400 mm specimens represent nearly 30% of the total volume of concrete used to produce three 150x150x600 mm samples, thus also reducing material costs, especially in works with large concrete production.
- Testing procedures for smaller specimens may remain constant with regard to tests conducted on standard specimens. In any case, only equivalent crack openings need to be measured. However, further work should be conducted to determine the influence of the test rate on the data acquisition and the test stability, especially after the strength drop at first crack.

Acknowledgements

The first author acknowledges the Spanish Ministry of Science, Innovation and Universities for the FPU13/04864 grant. The authors also want to express their gratitude to the Spanish Ministry of Economy, Industry and Competitiveness for the financial support through the SAES project (BIA2016-78742-C2-1-R).

REFERENCES

[1] G. H. Mahmud, Z. Yang, and A. M. T. Hassan, "Experimental and numerical studies of size effects of Ultra High Performance Steel Fibre Reinforced Concrete (UHPFRC) beams," *Constr. Build. Mater.*, vol. 48, pp. 1027–1034, Nov. 2013.

[2] K. Awinda, J. Chen, and S. J. Barnett, "Investigating geometrical size effect on the flexural strength of the ultra high performance fibre reinforced concrete using the cohesive crack model," *Constr. Build. Mater.*, vol. 105, pp. 123–131, 2016.

[3] D. Y. Yoo, N. Banthia, S. T. Kang, and Y. S. Yoon, "Size effect in ultra-high-performance concrete beams," *Eng. Fract. Mech.*, vol. 157, pp. 86–106, 2016.

[4] D.-Y. Yoo, N. Banthia, J.-M. Yang, and Y.-S. Yoon, "Size effect in normal- and high-strength amorphous metallic and steel fiber reinforced concrete beams," *Constr. Build. Mater.*, vol. 121, pp. 676–685, 2016.

[5] C. G. Hoover and Z. P. Bažant, "Cohesive crack, size effect, crack band and work-of-fracture models compared to comprehensive concrete fracture tests," *Int. J. Fract.*, vol. 187, no. 1, pp. 133–143, 2014.

[6] RILEM TC 162-TDF, "Final recommendation of RILEM TC 162-TDF: Test and design methods for steel fibre reinforced concrete sigma-epsilon-design method," *Mater. Struct.*, vol. 36, no. 262, pp. 560–567, Aug. 2003.

[7] A. Blanco, P. Pujadas, A. de la Fuente, S. Cavalaro, and A. Aguado, "Application of constitutive models in European codes to RC–FRC," *Constr. Build. Mater.*, vol. 40, pp. 246–259, Mar. 2013.

[8] International Federation for Structural Concrete, *fib Model Code for Concrete Structures 2010*. 2010.

[9] A. Blanco, S. Cavalaro, A. de la Fuente, S. Grünewald, C. B. M. Blom, and J. C. Walraven, "Application of FRC constitutive models to modelling of slabs," *Mater. Struct.*, vol. 48, no. 9, pp. 2943–2959, Sep. 2015.

[10] A. Blanco, P. Pujadas, A. de la Fuente, S. H. P. Cavalaro, and A. Aguado, "Assessment of the fibre orientation factor in SFRC slabs," *Compos. Part B Eng.*, vol. 68, pp. 343–354, Jan. 2015.

[11] M. Bastien-Masse, E. Denarié, and E. Brühwiler, "Effect of fiber orientation on the in-plane tensile response of UHPFRC reinforcement layers," *Cem. Concr. Compos.*, vol. 67, pp. 111–125, 2016.

[12] M. G. Alberti, A. Enfedaque, and J. C. Gálvez, "On the prediction of the orientation factor and fibre distribution of steel and macro-synthetic fibres for fibre-reinforced concrete," *Cem. Concr. Compos.*, vol. 77, pp. 29–48, Mar. 2017.

[13] AFGC, "Ultra high performance fibre-reinforced concrete. Recommendations," Association Française de Génie Civil, 2013.

[14] CEN, "EN 14651:2007. Test method for metallic fibre concrete. Measuring the flexural tensile strength (limit of proportionality (LOP), residual)." Brussels, 2007.

[15] R. Montaignac, B. Massicotte, and J.-P. Charron, "Design of SFRC structural elements: flexural behaviour prediction," *Mater. Struct.*, vol. 45, no. 4, pp. 623–636, Oct. 2011.

[16] M. di Prisco, M. Colombo, and D. Dozio, "Fibre-reinforced concrete in fib Model Code 2010: principles, models and test validation," *Struct. Concr.*, vol. 14, no. 4, pp. 342–361, Dec. 2013.

[17] F. Di Carlo, A. Meda, and Z. Rinaldi, "Design procedure for precast fibre-reinforced concrete segments in tunnel lining construction," *Struct. Concr.*, vol. 17, no. 5, pp. 747–759, Dec. 2016.

[18] G. Giaccio, J. M. Tobes, and R. Zerbino, "Use of small beams to obtain design parameters of fibre reinforced concrete," *Cem. Concr. Compos.*, vol. 30, no. 4, pp. 297–306, Apr. 2008.

[19] A. de la Fuente, R. C. Escariz, A. D. de Figueiredo, C. Molins, and A. Aguado, "A new design method for steel fibre reinforced concrete pipes," *Constr. Build. Mater.*, vol. 30, pp. 547–555, May 2012.

[20] A. de la Fuente, A. Aguado, C. Molins, and J. Armengou, "Numerical model for the analysis up to failure of precast concrete sections," *Comput. Struct.*, vol. 106–107, pp. 105–114, Sep. 2012.

[21] L. Liao, A. de la Fuente, S. Cavalaro, and A. Aguado, "Design procedure and experimental study on fibre reinforced concrete segmental rings for vertical shafts," *Mater. Des.*, vol. 92, pp. 590–601, Feb. 2016.

[22] B. Mobasher, M. Bakhshi, and C. Barsby, "Backcalculation of residual tensile strength of regular and high performance fiber reinforced concrete from flexural tests," *Constr. Build. Mater.*, vol. 70, pp. 243–253, 2014.

[23] B. Mobasher, Y. Yao, and C. Soranakom, "Analytical solutions for flexural design of hybrid steel fiber reinforced concrete beams," *Eng. Struct.*, vol. 100, pp. 164–177, 2015.

[24] D. Y. Yoo and Y. S. Yoon, "Structural performance of ultra-high-performance concrete beams with different steel fibers," *Eng. Struct.*, vol. 102, pp. 409–423, 2015.

[25] J. Á. López, P. Serna, J. Navarro-Gregori, and E. Camacho, "An inverse analysis method based on deflection to curvature transformation to determine the tensile properties of UHPFRC," *Mater. Struct.*, vol. 48, no. 11, pp. 3703–3718, 2015.

[26] J. Á. López, P. Serna, J. Navarro-Gregori, and H. Coll, "A simplified five-point inverse analysis method to determine the tensile properties of UHPFRC from unnotched four-point bending tests," *Compos. Part B Eng.*, vol. 91, pp. 189–204, Apr. 2016.

[27] D. Y. Yoo and Y. S. Yoon, "A Review on Structural Behavior, Design, and Application of Ultra-High-Performance Fiber-Reinforced Concrete," *Int. J. Concr. Struct. Mater.*, vol. 10, no. 2, pp. 125–142, 2016.

[28] K. Wille, S. El-Tawil, and a. E. Naaman, "Properties of strain hardening ultra high performance fiber reinforced concrete (UHP-FRC) under direct tensile loading," *Cem. Concr. Compos.*, vol. 48, pp. 53–66, Apr. 2014.

[29] E. Ghafari, H. Costa, E. Júlio, A. Portugal, and L. Durães, "The effect of nanosilica addition on flowability, strength and transport properties of ultra high performance concrete," *Mater. Des.*, vol. 59, pp. 1–9, Jul. 2014.

[30] CEN, "EN 12390-3. Testing hardened concrete. Part 3: Compressive strength of test specimens." Brussels, 2009.

[31] CEN, "EN 12390-13:2014. Testing hardened concrete – Part 13: Determination of secant modulus of elasticity in compression." Brussels, 2014.

[32] C. G. Hoover, Z. P. Bažant, J. Vorel, R. Wendner, and M. H. Hubler, "Comprehensive concrete fracture tests: Description and results," *Eng. Fract. Mech.*, vol. 114, pp. 92–103, 2013.

[33] N. Trivedi, R. K. Singh, and J. Chattopadhyay, "Investigation on fracture parameters of concrete through optical crack profile and size effect studies," *Eng. Fract. Mech.*, vol. 147, pp. 119–139, 2015.

[34] K. Kirane and Z. P. Bazant, "Size effect in Paris law and fatigue lifetimes for quasibrittle materials: Modified theory, experiments and micro-modeling," *Int. J. Fatigue*, vol. 83, pp. 209–220, 2016.

[35] L. G. Sorelli, A. Meda, and G. A. Plizzari, “Bending and Uniaxial Tensile Tests on Concrete Reinforced with Hybrid Steel Fibers,” *J. Mater. Civ. Eng.*, vol. 17, no. 5, pp. 519–527, Oct. 2005.

[36] M. N. Soutsos, T. T. Le, and a. P. Lampropoulos, “Flexural performance of fibre reinforced concrete made with steel and synthetic fibres,” *Constr. Build. Mater.*, vol. 36, pp. 704–710, Nov. 2012.

[37] D.-Y. Yoo, H.-O. Shin, J.-M. Yang, and Y.-S. Yoon, “Material and bond properties of ultra high performance fiber reinforced concrete with micro steel fibers,” *Compos. Part B Eng.*, vol. 58, pp. 122–133, 2014.

[38] M. Pająk and T. Ponikiewski, “Flexural behavior of self-compacting concrete reinforced with different types of steel fibers,” *Constr. Build. Mater.*, vol. 47, pp. 397–408, Oct. 2013.

[39] D. Y. Yoo, S. Kim, G. J. Park, J. J. Park, and S. W. Kim, “Effects of fiber shape, aspect ratio, and volume fraction on flexural behavior of ultra-high-performance fiber-reinforced cement composites,” *Compos. Struct.*, vol. 174, pp. 375–388, 2017.

[40] N. Buratti, C. Mazzotti, and M. Savoia, “Post-cracking behaviour of steel and macro-synthetic fibre-reinforced concretes,” *Constr. Build. Mater.*, vol. 25, no. 5, pp. 2713–2722, May 2011.

[41] M. G. Alberti, A. Enfedaque, J. C. Gálvez, and V. Agrawal, “Reliability of polyolefin fibre reinforced concrete beyond laboratory sizes and construction procedures,” *Compos. Struct.*, vol. 140, pp. 506–524, Apr. 2016.

[42] R. Lameiras, J. A. O. Barros, and M. Azenha, “Influence of casting condition on the anisotropy of the fracture properties of Steel Fibre Reinforced Self-Compacting Concrete (SFRSCC),” *Cem. Concr. Compos.*, vol. 59, pp. 60–76, 2015.

[43] L. Vandewalle, “Hybrid fiber reinforced concrete,” in *Measuring, Monitoring and Modeling Concrete Properties*, 2006, pp. 77–82.

[44] D. L. Nguyen, D. J. Kim, G. S. Ryu, and K. T. Koh, “Size effect on flexural behavior of ultra-high-performance hybrid fiber-reinforced concrete,” *Compos. Part B Eng.*, vol. 45, no. 1, pp. 1104–1116, Feb. 2013.

[45] D.-Y. Yoo, N. Banthia, S.-T. Kang, and Y.-S. Yoon, “Size effect in ultra-high-performance concrete beams,” *Eng. Fract. Mech.*, 2016.

[46] Z. Wu, C. Shi, W. He, and L. Wu, “Effects of steel fiber content and shape on mechanical properties of ultra high performance concrete,” *Constr. Build. Mater.*, vol. 103, pp. 8–14, 2016.

[47] B. Zhou and Y. Uchida, “Influence of flowability, casting time and formwork geometry on fiber orientation and mechanical properties of UHPFRC,” *Cem. Concr. Res.*, vol. 95, pp. 164–177, 2017.

[48] R. Yu, P. Spiesz, and H. J. H. Brouwers, “Mix design and properties assessment of Ultra-High Performance Fibre Reinforced Concrete (UHPFRC),” *Cem. Concr. Res.*, vol. 56, pp. 29–39, Feb. 2014.

[49] T. A. Söylev and T. Özturan, “Durability, physical and mechanical properties of fiber-reinforced concretes at low-volume fraction,” *Constr. Build. Mater.*, vol. 73, pp. 67–75, 2014.

[50] R. Zerbino, J. M. Tobes, M. E. Bossio, and G. Giaccio, “On the orientation of fibres in structural members fabricated with self compacting fibre reinforced concrete,” *Cem. Concr. Compos.*, vol. 34, no. 2, pp. 191–200, Feb. 2012.

[51] J. S. Lawler, D. Zampini, and S. P. Shah, “Microfiber and Macrofiber Hybrid Fiber-Reinforced Concrete,” *J. Mater. Civ. Eng.*, vol. 17, no. 5, pp. 595–604, 2005.

[52] D. Y. Yoo, Y. S. Yoon, and N. Banthia, “Predicting the post-cracking behavior of normal- and high-strength steel-fiber-reinforced concrete beams,” *Constr. Build. Mater.*, vol. 93, pp. 477–485, 2015.